

Stephan Domayer, Sebastian Apprich, Benjamin Schmitt,
Oliver Bieri, and Siegfried Trattnig

Introduction

Much of the difficulty in studying OA and the efficacy of interventions is due to the current limitations in the use of plain radiographs, which are currently deemed the gold standard for noninvasive assessment of clinical OA. Often, changes such as joint space narrowing or formation of osteophytes, which can be detected on radiographs, manifest at late stage [1], when disease modifying therapies including surgery and/or drug treatment may already be ineffective. Sensitive techniques that could detect early OA and reliably monitor its progression would help to identify patients who may benefit from joint preserving interventions, to reduce the number of patients requiring arthroplasty or at least delaying the need of total hip arthroplasty (THA). In addition, the identification of patients who are likely to progress rapidly would be particularly useful when designing clinical trials. Therefore, an early diagnosis of cartilage degeneration and a sensitive, noninvasive diagnostic tool are highly desirable.

In morphologic images, the signal intensity of each pixel results from a vast number of both intrinsic and extrinsic factors. The principle extrinsic factors are field strength, magnetic

field homogeneity and the general hard- and software setup of the MR scan. The principle intrinsic parameters in clinical imaging are T1, T2, and proton density, which has led to the terms T1-, T2-, and proton-weighted images.

The basic principle of biochemical MR imaging is that single intrinsic parameters of the cartilage tissue are assessed by the use of dedicated sequences. This allows for a more specific description of the tissue, as distinct MR parameters directly correspond to specific properties of the cartilage tissue.

For these reasons, there is a topical interest in advancing non-contrast biochemical imaging techniques sensitive to changes at the molecular level of articular cartilage, such as T2 mapping, T2* mapping, T1 rho, diffusion-weighted Imaging (DWI), CEST, or Sodium. A number of studies showed very promising first results over the recent years for quantitative, non-contrast cartilage MR imaging for early detection of cartilage degeneration. However, owing to the availability of high-quality knee coils the majority of work was based on the knee joint cartilage. With a few exceptions, literature reporting on the feasibility of quantitative “biochemical” non-contrast MR imaging of the hip joint is lacking. As the hip joint cartilage is a relatively thin and curved structure, it makes great demands on the investigator and the available hardware and sequences for valid imaging. Existing evaluation methods suffer from insufficient spatial resolution, prolonged acquisition times, and low signal-to-noise ratio (SNR). New 3.0 T and 7.0 T magnetic

S. Trattnig (✉)

Department of Radiology, Medical University of Vienna,
Währinger Gürtel 18-20, Vienna 1090, Austria
e-mail: siegfried.trattnig@meduniwien.ac.at

resonance scanners have decreased the scan time by a factor of 2–3, improved the SNR, the spatial resolution, and allow thinner slice thickness. With concurrent improvement in coil-technology and optimization of imaging protocol, quantitative MR imaging has a high potential for future human in vivo imaging and may overcome the present restrictions in imaging of the hip cartilage.

T2 Mapping

The spatial variation of T2 values across cartilage was first reported in 1989 [2]. In normal cartilage, T2 shows a subtle decrease from the subchondral lamina to the deep layer, and subsequently a steady increase towards the surface.

Several aspects contribute to this phenomenon. In the deep zone, the collagen fibers run anisotropically perpendicular to subchondral bone; there is a reduced mobility of water protons, and therefore reduced T2 relaxation time values. In the superficial zone, the collagen fibers are randomly oriented which leads to an increase of T2 values from the deep to superficial zone in normal hyaline cartilage.

Additionally, the dipolar coupling of collagen-associated water is minimum at 54.7° to the static magnetic field, which leads to increased T2 (magic angle effect) [3–5]. This phenomenon depends on the orientation of the cartilage to the static magnetic field, and therefore is an extrinsic factor that can substantially alter T2 measurements.

Free water leads to a prolongation of T2 in general; as a consequence, a loss of proteoglycan content and subsequently increased water is deemed to lead to increased T2 in cartilage.

Several investigators have explored the relevance of these factors for T2 of cartilage particularly with regard to the magic angle effect.

Grunder et al. [6] reported a 300 % increase of T2 when the sample was oriented at 55° to the magnetic field in an in vitro setting at 7.1 T. Mosher et al. [7] evaluated the relevance of this phenomenon for in vivo T2 measurements in the knee in a clinical setting. They found that the magic angle effect contributed less than

expected to variations in T2. When oriented at 55° , T2 increased 8.6 % at a normalized distance of 0.3 from the bone 18.3 % at 0.6, and 29.1 % near the surface. However, at all orientations the zonal variation of T2 was clearly present. In conclusion, the increase of free water in the superficial zone during the absence of compression and conversely, a decrease of T2 of the superficial layer under compression was deemed to be more accountable for regional differences of T2 (especially joint loading areas versus the posterior femoral condyle) than the orientation to the magnetic field. They concluded the magic angle effect was unlikely to account for significant regional differences in clinical imaging. Nieminen et al. [3] compared polarized light microscopy and optical density of safranin O analysis with T2 in order to evaluate the morphologic parameters that determine T2 and concluded that proteoglycan content does not contribute significantly to T2, but that free water collagen content and the architecture of the collagen fibers are reflected in T2.

As a consequence, T2 mapping has found widespread application in in vivo MRI studies on osteoarthritis. Based on the hypothesis that the loss of proteoglycan will result in an increase of free water, increased T2 was expected to be a marker for osteoarthritis. However, there is data demonstrating unchanged T2 or decreased T2 in degraded cartilage in vitro and in clinical T2 images [2]. A possible explanation is the creation of collagen cleavage sites in the course of degradation that interact with free water, decreasing T2.

A moderate relationship between age and T2 of the cartilage layer has been reported [8]; however, the range of individual cartilage T2 is such that no predictive value can be deduced at this time.

In contrast, the technique has proven immensely useful for the assessment of surgical cartilage repair techniques. A basic condition for cartilage repair is that the adjacent articular cartilage is intact. Under this assumption, T2 values of repair tissue can be compared to healthy cartilage in each patient, which substantially differentiates the application of T2 in cartilage repair from monitoring OA.

A horse model study by White et al. [4] demonstrated that normal hyaline cartilage and cartilage repair tissue could be differentiated by zonal T2 mapping. Arthroscopic osteochondral autograft transplantation (OAT) and MFX were performed and evaluation of zonal T2 variation showed a characteristic distribution across the depth of the cartilage in control and OAT sites, with low T2 values near the subchondral bone and higher T2 values near the cartilage surface [4]. In contrast, no zonal variation was found within MFX repair tissue. Correlation with histology and collagen structural anisotropy as assessed by polarized light microscopy demonstrated a near perfect specificity of T2. OAT and normal hyaline cartilage sites illustrated a normal zonal collagen organization, whereas MFX showed disorganized fibrous reparative tissue [4].

Using quantitative global T2 mapping of patients at different postoperative intervals after MACT surgery, significantly higher T2 values were found in cartilage repair tissue in the early stage (3–13 months) after surgery in an intra-individual comparison with native hyaline cartilage [9]. Furthermore, a decrease in repair tissue T2 values was observed over time, with the T2 values becoming similar to native healthy cartilage. This finding was in agreement with a study by Kurkijarvi et al. [10] who reported T2 of the repair tissue and normal hyaline in the range of 60 and 50 ms at 1.5 T, respectively, in 10 patients at 10–15 months after ACI surgery. The zonal variation of repair tissue [9] has been demonstrated by the analysis of the T2 line profiles showing the variation of T2 values from the subchondral bone to cartilage surface. With increasing postoperative interval the shape of the T2 line profiles (and the calculated T2 line profile values) was found to become similar to the reference healthy cartilage sites [9]. A direct comparison of cases after MFX and after MACT in the knee has demonstrated that MFX yields repair tissue with significantly lower T2 than MACT; significant differences could be demonstrated in terms of the degree of zonal variation. Whereas there is no spatial variation of T2 in MFX repair tissue, a subtle increase was found after MACT, albeit not comparable to the

native adjacent cartilage [11]. With regard to the inherently large variation of T2 among individuals, it has proven to be useful to describe the T2 properties of the repair tissue relative to the adjacent reference cartilage. The relative T2 relaxation time ($rT2$) is calculated from the global T2 values ($rT2 = T2 \text{ of repair tissue} / T2 \text{ of reference cartilage}$) [5].

A direct correlation of $rT2$ and the clinical outcome showed there was a relationship between the repair tissue T2 properties and the clinical outcome. Cases that have repair tissue with T2 properties that are equal to the reference are more likely to do well.

The technique could be transferred to the ankle, albeit with limitations. Due to the thin cartilage layers of the ankle, it was not feasible to optimize the protocol for a zonal assessment of the cartilage layers. However, it was possible to assess $rT2$ after MFX and after MACT of the ankle. $rT2$ was 1.00 ± 0.20 (0.72–1.36) in a series of 14 cases after MFX and 0.85 ± 0.21 (0.49–1.26) in a series of 8 cases after Hyalograft C, and in another series of 12 cases after MACT $rT2$ was 1.05 (50.1 ± 8.0 ms in the RT and 47.6 ± 9.3 ms in the reference cartilage) [12–14]. Other than in the knee, the water and collagen content was similar to the reference cartilage after both treatment modalities. It should, however, be noted that a zonal analysis was not feasible at 3 T, mainly due to the lower SNR. A subsequent study at 7 T demonstrated that other than in the knee, MFX of the ankle results in organized RT and may be particularly suited for the treatment of cartilage defects of the ankle, as there was a significant increase of T2 towards the surface in the repair tissue (OAC 7T).

Methodological Considerations

Spin echo imaging with separate acquisitions for each TE is considered the gold standard for T2 measurement, but it is not feasible in clinical routine due to acquisition time. Multislice multiecho spin echo (MESE) sequences provide faster imaging, but there are some aspects to be considered with regard to accuracy.

Multislice imaging requires slice-selective refocusing pulses that will produce transitional regions at slice boundaries. Resulting imperfect refocusing and therefore stimulated echo contribution in fast spin echo introduce mixed T1 and T2 contrast to the image. A detailed comparison of a single echo spin echo with a multiecho spin echo sequence in agarose phantoms with T2 values in the range of articular cartilage and differing T1 values at 1.5 T [15] yielded an error of 10 % that increased with longer T1 as the later echoes had increased signal due to the stimulation by the imperfect refocusing pulses. When the first echo was dropped from the curve fitting, the error decreased considerably to 0.3–5.2 %; elimination of the first pulse improved T2 accuracy because the decay rate of mixed T1/T2 was similar to pure T2. Still, a comparison in volunteers showed the error was still between –11.6 and 16.9 %. Even though the qualitative T2 pattern of cartilage was comparable with the different sequences, absolute T2 differed considerably.

Furthermore, magnetization transfer contrast created by refocusing pulses for other slices diminishes signal intensity in cartilage and can thus impair the accuracy of T2 measurement [15]. Additional factors that may affect T2 quantification are field inhomogeneities and insufficient sampling of the T2 decay curve [16].

A comparative phantom study by Pai et al. [16] at 3 T regarding sequence-dependent T2 quantification yielded the MESE sequence had the best accuracy; however, the measures in volunteers confirmed an increase in T2 measured by MESE compared to SE T2 in accordance with Maier et al.. With regard to the phantom study, the authors concluded that rather a T2 underestimation of the SE than an overestimation by the MESE was found in cartilage.

Regarding the reproducibility of T2, coefficients of variance in the range of 0.1–2.8 % in phantoms and 5.3 % in cartilage have been reported for a MESE sequence; a comparison with the other sequences showed that the average coefficient of variance was lowest in the MESE (1.3 %). In other volunteer studies, the relative precision errors for T2 are reported to range

between 2.76 and 5.37 % at 1.5 T, and a further comparison of T2 mapping at 1.5 T and 3 T demonstrated comparable coefficient of variation at either field strength in the same resolutions, suggesting good discriminatory power of the technique [17, 18].

Regarding the magic angle effect, there remains considerable uncertainty regarding its influence on absolute T2. At least in cartilage repair assessment the phenomenon can be considered in the ROI analysis by comparing the repair tissue to a reference area with the same orientation to the static magnetic field.

In summary, a considerable error of absolute T2 values has to be expected when using different T2 mapping protocols. This can be aggravated by the use of different coils, and obviously, T2 values obtained at different field strengths cannot be compared. Additionally, there seems to be a large variability of T2 in healthy cartilage. It is therefore unlikely that thresholds can be defined to distinguish between normal cartilage and OA. The strength of the technique lies in the assessment of the zonal collagen network organization of cartilage and cartilage repair tissue.

T2* Mapping

Within a clinical imaging protocol, T2 mapping is still limited. The long echo trains of the spin echo technique, needed to accurately characterize the cartilage T2 decay curve, contribute to prolonged acquisition times (TA), typically exceeding 10 min for complete coverage of full joints. The 2D-acquisition precludes reformatting the data into 3D surface maps and requires reliable positioning to achieve reproducible results. Furthermore, the inherent variability in the 180° refocusing pulses leads to errors in T2 estimates as a result of the contribution from simulated echos and magnetization transfer [19].

T2* relaxation time mapping, based on a non-contrast gradient-echo (GRE) sequence, might be an alternative biochemical marker. This technique combines the potential of short scan time

and high isotropic resolution of thin cartilage layers due to high signal-to-noise ratio and three-dimensional (3D) imaging. This is especially important concerning the complex hip joint with its curved surface and thin cartilage. In morphological MRI studies, radial evaluation of the hip cartilage in a clockwise manner from anterior to posterior and perpendicular around the femoral neck has become the gold standard for hip imaging. Isotropic 3D T2* data sets and the capability of multi-planar reconstruction allow for quantitative evaluation in the same manner [20].

In contrast to standard T2-weighted spin echo techniques, 3D-GRE-sequences lack the 180° refocusing pulse. As a consequence, time-independent inhomogeneities of the external magnetic field (B_0) and intrinsic factors like susceptibility artifacts contribute to a faster dephasing of the spins, resulting in an overall signal decay that is faster than described by T2 (T2*).

The T2* relaxations time is related to T2 as follows: $1/T2^* = 1/T2 + \gamma\Delta B_0$ where γ represents the gyromagnetic ratio and ΔB_0 defines the difference in strength of the locally varying field. Assuming the applied static magnetic field (B_0) is uniform and constant over the region of interest, then T2* will be influenced by both the transverse relaxation (T2) and by the local susceptibility fields. Such local fields can operate at the macroscopic level, i.e., at the bone–cartilage interface, or at the microscopic level associated with the underlying microstructure of proteoglycans and collagen fibers within the cartilage. The lack of radiofrequency refocusing pulses substantially decreases the contribution of magnetization transfer to cartilage contrast, and thus, may lead to differences in sensitivity of T2* and T2 to changes in the collagen content in cartilage.

Typical T2* mapping sequences for the cartilage use 6–8 TE's in the range of 5–50 ms to measure the T2* decay. Subsequently, T2* maps are generated ideally throughout an inline processing package, which utilizes a nonlinear least square fitting routine, to avoid time-consuming post-processing.

A further important point which should be considered within a setting of clinical studies is the placement of the T2/T2* mapping sequence at the end of the MR-protocol. Related to T2 mapping studies with unloading of the knee joint [21, 22], a recent study on T2* mapping of the hip joint has shown the effect of rehydration of the cartilage to be of crucial importance for designing an MR-protocol in patients with FAI [23].

A limitation of T2* mapping within a clinical setting is the application of this technique in the presence of metallic particles as a result of surgery due to the greater sensitivity to susceptibility-included artifacts. Another factor that must be considered, in particular when assessing the spherical shape of the hip joint cartilage, is the magic angle effect. It is characterized by an increase of T2 (and therefore T2*) values when the cartilage is orientated at ~56° to the main magnetic field and the dephasing effect of parallel-oriented dipolar interactions of protons in water molecules binding to collagen is minimized. However, the dependency of T2* on collagen fiber orientation has to be systematically evaluated in future studies on articular cartilage.

In theory, injury to the calcified cartilage zone, or changes in the cartilage microstructure could lead to changes in the magnetic susceptibility of the tissue that could be exploited using T2* mapping.

Chemical Exchange Saturation Transfer

Chemical exchange saturation transfer (CEST) is a ^1H MR imaging (MRI) technique that enables visualization of chemical exchange processes between protons bound to solutes and surrounding bulk water molecules [24–26]. To induce a CEST contrast, the off-resonant solute protons are labeled by a saturation radiofrequency (RF) pulse and the label is then transferred to bulk water by chemical exchange. The magnitude of the subsequent reduction of

bulk water signal depends consequently on the dynamics of chemical exchange as well as on the ratio of exchangeable solute protons to bulk water protons [27]. The rate constant of chemical exchange (k), i.e., the velocity of chemical exchange, is principally influenced by the pH value and the temperature within the exchange environment. If the latter two parameters can be assumed to be distributed homogeneously in tissue and maintained at a constant level during one experiment, the CEST effect will be a surrogate marker of the concentration of a certain solute molecule in tissue. In order for a solute molecule to be considered suitable as an endogenous CEST agent, it must carry labile protons that exchange with bulk water at exchange rates that fulfill the condition $k < \Delta\omega$; where $\Delta\omega$ is the resonance offset of the solute protons to the water protons in $[s^{-1}]$ [27].

Glycosaminoglycan-dependent chemical exchange saturation transfer (gagCEST) imaging was introduced by Ling et al. as a CEST imaging method that produces a contrast based exclusively on the chemical exchange between endogenous solute GAG molecules and surrounding bulk water [28]. This is of interest because GAGs are major constituents of the extracellular matrix of different connective tissues, such as cartilage, intervertebral discs (IVD) and menisci, and they are responsible for the biomechanical properties of these tissues [29–31]. Since pH value and temperature are relatively stable within connective tissues, variations of gagCEST signals were shown to correlate linearly with sodium content in cartilage assessed by ^{23}Na MRI [28], which, in turn, is a reference method for assessment of GAG content in cartilage [32–35]. In order to evaluate the potential of gagCEST imaging as a noninvasive tool for monitoring of cartilage GAG content, two initial studies were conducted in patients after cartilage repair surgeries [36, 37]. Previous studies had shown that cartilage repair tissue is likely to exhibit lower GAG content than native cartilage [38–40]. This finding, in combination with a usually well-defined repair area, makes repair tissue an ideal model system for evaluation of gagCEST or other possibly GAG-sensitive imaging techniques [41–43]. Both aforementioned

gagCEST studies were conducted on human 7 T MR systems and gagCEST results were compared to sodium imaging as a reference for GAG content. The first study focused on patients, which had undergone microfracturing (MFx) therapy or matrix-associated chondrocyte transplantation (MACT). Both GAG-sensitive methods showed a strong correlation between each other and indicated significantly lower GAG content in repair tissue compared to native cartilage [37]. This result was confirmed in a second study that examined the long-term outcome of patients after autologous osteochondral transplantation (AOT) [36]. In the latter study, gagCEST and sodium imaging consistently showed reduced GAG content in repair sites. In addition to cartilage assessment, gagCEST imaging was used to investigate GAG content in IVDs [44, 45] and feasibility was demonstrated in healthy volunteers at 3 T. Both IVD studies showed different gagCEST signal intensities in nucleus pulposus compared to the annulus fibrosus as a result of the different GAG concentrations in these IVD compartments.

The common method for acquisition of a CEST dataset is to acquire multiple image datasets with presaturation at different offset frequencies (S_{Sat}) around the water resonance, and one reference dataset without saturation (S_0). This is regardless of the specific agent or resonance frequency that is evaluated to generate the desired CEST contrast. The normalized signal as a function of the presaturation offset (z -spectrum) can then be used to determine and quantify CEST effects, which are asymmetric with respect to the water resonance; i.e., a CEST effect appears either up- or downfield from water and can hence be extracted from the z -spectrum via analysis of its asymmetry with respect to the water resonance. Nevertheless, in vivo z -spectra are inherently asymmetric due to conventional magnetization transfer (MT) effects arising predominantly from solid-phase macromolecules. CEST effects are also masked by concomitant direct water saturation (“RF spill-over”) as a result of the bandwidth of the saturation pulses. This phenomenon is further emphasized if the resonance frequencies of the investigated exchangeable protons have only small chemical shift differences to bulk water protons. The

exchangeable protons of GAG molecules that are used to generate the gagCEST contrast, namely hydroxyl and amide protons, exhibit relatively small chemical shift offsets from bulk water protons. In particular, the labile $-NH$ protons resonate at $\Delta\omega = 3.2$ ppm offset from the water resonance and $-OH$ protons at $\Delta\omega = 0.9\text{--}1.9$ ppm ($\Delta \sim 114\text{--}241$ Hz at 3.0 T). Additionally, the exchange rates of the hydroxyl protons can be on the order of up to $1,000\text{ s}^{-1}$. Therefore, exchange rates may be in the intermediate to fast exchange regime at a magnetic field strength of 3.0 T ($k \geq \Delta\omega$), which makes the resonance signals difficult to resolve at 3.0 T. Although the situation improves considerably when switching to a field strength of 7.0 T, it is generally necessary to use tailored CEST acquisition and saturation strategies for gagCEST investigations. This means that time-efficient and narrowband saturation of CEST resonances must be enabled in addition to rapid signal readout after saturation.

Since multiple datasets are acquired in one gagCEST examination, it is mandatory for proper analysis of z -spectra to compensate for patient motion between acquisitions so the datasets recorded with different presaturation offsets are correctly aligned. Furthermore, correction of inhomogeneities of the static magnetic field, which can lead to severe miscalculation of CEST effects, has to be performed before analysis of z -spectra.

Several acquisition strategies have been proposed for gagCEST imaging, predominantly relying on 3D gradient-echo, or single-slice slice fast spin echo and GRE approaches [28, 37, 44–46]. While 3D acquisition techniques enable a more comprehensive overview of imaging volumes than single-slice techniques, they usually require longer scan times, which can be of concern for clinical routine. Additionally, in some joints where cartilage is thin compared to knee cartilage such as in the ankle or the hip, high spatial resolution is required for proper assessment of biochemical cartilage properties. However, gagCEST effects are in the order of 1–4 % of the bulk water signal at 3.0 T, and of 3–8 % at 7.0 T in healthy knee cartilage [37, 45]. Thus, high intrinsic image SNR is required to reliably detect and quantify gagCEST effects. Image

SNR in MRI can only be maintained by increasing the scan time when higher spatial resolution is desired. Consequently, the maximum achievable spatial resolution for gagCEST imaging will certainly be limited by the scan time available for an exam. The acquisition strategy proposed by Schmitt et al. [37] was based on a 3D GRE approach and sampled z -spectra with 13 points from $\Delta\omega = -2.6$ to 2.6 ppm with a voxel resolution of $0.6 \times 0.6 \times 3.3\text{ mm}^3$ in 11:24 min (measurement at 7.0 T, full knee coverage).

Another limitation of gagCEST imaging may be the observed intra-individual differences of absolute gagCEST values, which impairs comparability of results between individuals. The differences are attributed to the fact that gagCEST signal intensities depend strongly on the absolute water content of tissue and tissue T_2 relaxation times. Both parameters can vary considerably among individuals and will thus influence absolute CEST values unless a proper normalization is applied or correction factors are introduced.

Imaging of Cartilage Diffusion

Molecular diffusion, also known as Brownian motion (see Einstein–Smoluchowski relation [47, 48]), refers to the random movement of small particles (atoms or molecules) in a homogeneous medium by thermal energy, captured by the so-called diffusion coefficient, D , measuring of the diffusivity or mobility of the particles. In biological tissues, however, water is diffusing not only in a solvent containing macromolecules but, typically, for the time periods involved in MRI also in a complex microstructure having different biophysical and biochemical properties. In that case, the notion of an apparent diffusion coefficient (frequently termed ADC) is used. Furthermore, diffusion is generally not directionally uniform, as it would be for water in a bucket of water, but directionally sensitive, that is anisotropic. Especially in highly oriented structures, such as muscle or nerve fibers, the apparent diffusion coefficient along different directions can differ by up to a factor of 3. As a result, for the

characterization of water diffusion in tissues, the diffusion coefficient is no longer a scalar value but a three-by-three matrix (or tensor) representing the different directional sensitivities. Complete characterization of the diffusion tensor is a demanding task, and frequently diffusion effects are confined into a simple orientational averaged mean diffusivity, $\langle D \rangle$, calculated from the trace of the diffusion tensor. Typical values for the mean diffusivity of water in biological tissues are in the range of $0.7 \times 10^{-3} \text{ mm}^2/\text{s}$ for human brain, $1.3 \times 10^{-3} \text{ mm}^2/\text{s}$ for cartilage, and up to $3.0 \times 10^{-3} \text{ mm}^2/\text{s}$ for fluids.

In MRI, Diffusion Weighted Imaging (DWI) refers to a class of methods able to probe the diffusivity of water in biological tissues, *in vivo* and noninvasively. The essence to any DWI experiment is that in the presence of a magnetic gradient field diffusion causes random phase shifts in the transverse magnetization of each water molecule leading within an imaging voxel to a loss of net magnetization, as compared to the static case. Diffusion measurements were already described by Stejskal and Tanner in 1965 for NMR [49] and entered MRI in the mid-1980s [50–52]. Since then, water diffusion MRI has proven to be a highly sensitive and specific parameter, mainly for the detection of neurological disorders. As a result, contemporary DWI sequences are typically single shot techniques consisting of a diffusion-sensitizing preparation part (a spin echo or stimulated echo) followed by an echo planar imaging (EPI) signal readout. EPI sequences have the major advance that they are highly insensitive to bulk motion and are probably the fastest imaging sequences available, but application to the musculoskeletal (MSK) system is demanding: typically, T_2 of cartilage or muscle is about a factor of 2–3 shorter than the one of brain tissue, leading to a prominent signal loss, especially in combination with the high resolution and large field-of-view requirement of MSK applications. In addition, strong magnetic field inhomogeneities from bone-tissue interfaces lead to severe image distortions that may need retrospective correction. As a result, especially steady state DWI sequences

have gained increased importance for MSK imaging due to their excellent spatial resolution and high diffusion sensitivity [53–55].

Diffusion sensitivity to steady state free precession (SSFP) sequences is commonly induced by large gradient crusher moments, leading to a steady state signal that is composed of many different transverse and longitudinal echo paths or modes; including also stimulated echoes. For DWI, especially the “Echo” (that is the refocused signal immediately preceding the RF pulse) turns out to be very sensitive to diffusion representing a unique alternative to common EPI-based DWI, whereas the “FID” signal (that is the signal immediately following the RF pulse) is generally not used, since its sensitivity to diffusion is quite low. Over the years, several models have been developed for the description of diffusion effects in SSFP [56–60], all of them being based on the seminal work of Kaiser, Bartholdi, and Ernst (KBE) [56]. In MRI, besides semi-empirical approaches, such as the one presented by LeBihan [57], the extension of the KBE ansatz to pulsed gradient SSFP by Wu and Buxton [59, 60] is generally well accepted and several research groups have examined the effect of a constant crusher gradient for DWI with SSFP-Echo (also known as PSIF, CE-FAST) [53–55, 61, 62].

Diffusion quantification with SSFP-Echo, however, is complicated by manifold echo contributions leading to a complicated signal dependency on relaxation times (T_1 and T_2), as well as on sequence parameters, such as the repetition time (TR) or the flip angle (α). Quantification was, nevertheless, shown to be feasible *in vivo* in the fast-transverse-decay regime (that is for repetition times $\text{TR} > T_2$), provided that T_1 can be estimated [54]. In this regime, only the shortest coherence pathways contribute to the signal and thus signal attenuation from diffusion becomes independent of T_2 [60]. Clinically, however, this limit seems of rather low interest since signal-to-noise and scanning efficiency is substantially reduced from the required long echo times ($\text{TE} \sim 2 \times \text{TR} \gg T_2$) and far from what

is considered to be optimal. This is in contrast to SSFP-Echo DWI in the very-rapid-pulsing regime (that is for $TR \ll T_2$), offering substantially increased signal-to-noise and sequence efficiency. This regime has recently shown great promise for characterization of cartilage function and repair [63–65], but quantification of diffusion effects was complicated not only by the aforementioned pronounced sensitivity on relaxation but also due to a failure of the common Wu-Buxton model (and thus the KBE ansatz) in this limit [66]. This issue can be resolved by using an accurate SSFP diffusion model, as proposed by Freed et al. in the context of spectroscopy [67], and only recently, it was shown that for low flip angles, diffusion sensitivity in the SSFP-Echo arises mainly from longitudinal modes, effectively decreasing its relaxation sensitivity to T_1 only, similar to what can be achieved in the fast-transverse-decay regime. As a result, a new approach for quantitative SSFP-Echo DWI in the very-rapid-pulsing regime was proposed [66], allowing to probe diffusion properties of human articular cartilage in the knee joint in a clinical setup (Fig. 2.1)

A completely different approach for DWI with SSFP-Echo was proposed by Zur et al. [68], using bipolar rather than unipolar diffusion-sensitizing crusher gradients to reduce sensitivity to bulk motion. This concept was recently revisited and extended by Deimling [69], proposing a double-echo steady state (DESS) imaging technique for DWI with SSFP rather than a single echo method based on SSFP-Echo. Acquiring both primary SSFP modes with DESS, namely the Echo and the FID (also known as FISP, FAST, GRASS), offers the advance that diffusion effects are in combination with bipolar gradients and with respect to the Echo/FID signal ratio independent on relaxation times, as already noticed much earlier by Cho [70]. Unfortunately, however, bipolar gradient waveforms are not very diffusion-sensitive and thus generally require large moments and long repetition times.

Recently, a new and truly diffusion-weighted technique that is relaxation-independent SSFP

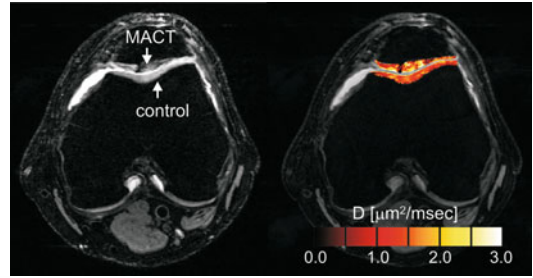


Fig. 2.1 In vivo axial sample image of a nondiffusion (*left*) and diffusion-weighted (*right*, averaged over three orthogonal directions) 3D SSFP-Echo scans with fused diffusivity map (using estimated T_1 information) of in vivo cartilage in the knee joint of a patient after matrix-associated autologous cartilage transplantation (MACT) at 3.0 T. A mean diffusivity of $1.42 \pm 0.24 \times 10^{-3} \text{ mm}^2/\text{s}$ was found for the control cartilage and $1.73 \pm 0.54 \times 10^{-3} \text{ mm}^2/\text{s}$ for the transplant (MACT). Scans were performed with $0.5 \times 0.5 \text{ mm}^2$ inplane resolution and 3 mm slice thickness; for other details, cf. [66]

technique was introduced based on a DESS approach using diffusion-sensitizing crusher moments [71]. It was shown that SSFP signal attenuation from diffusion becomes independent on relaxation with respect to the Echo-FID signal ratio, in complete analogy to what was observed by Cho et al. using bipolar gradients. As a result, quantitative SSFP DWI can be performed in the very-rapid-pulsing regime from two DESS scans, similar to what is proposed for SSFP-Echo but without the confounding influences of relaxation times, allowing high-resolution quantitative diffusion imaging of human articular cartilage in the knee joint at 3.0 T (see Fig. 2.2). Simultaneously, a similar approach for diffusion quantification was proposed by Staroswiecki et al. [72] allowing simultaneous estimation of T_2 and of the apparent diffusion coefficient from two DESS acquisitions with different crusher gradients and flip angles.

In summary, diffusion-sensitized SSFP, either based on the acquisition of the Echo only or on the double-echo approach using the FID to correct for relaxation time sensitivities in the Echo, have shown great promise for in vivo high-resolution

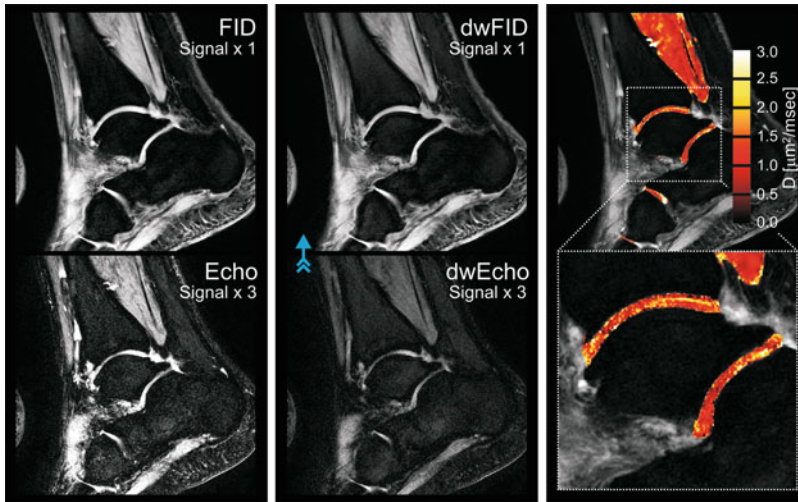


Fig. 2.2 High-resolution quantitative 3D DESS DWI of normal appearing cartilage in the ankle joint at 3.0 T. (Left) Sagittal nondiffusion-weighted DESS scan. (Middle) DESS scan with diffusion-sensitizing crusher moments along the direction indicated by the blue arrow. (Right) Fusion of the derived diffusion map

onto a conventional DESS image (derived from the nondiffusion-weighted DESS scan). For cartilage, a diffusivity of $D = 1.21 \pm 0.48 \times 10^{-3} \text{ mm}^2/\text{s}$ is found. Scans were performed with $0.4 \times 0.4 \text{ mm}^2$ inplane resolution and 3 mm slice thickness; for other details, cf. [71]

quantitative DWI of cartilage in 3D and within reasonable scan times in a clinical setup. Sensitivity to bulk motion, however, is a major issue with diffusion-sensitized SSFP, and proper fixation seems not only mandatory but has carefully to be conducted prior to any measurement.

References

- Locher S, Werlen S, Leunig M, Ganz R. [Inadequate detectability of early stages of coxarthrosis with conventional roentgen images]. *Z Orthop Ihre Grenzgeb.* 2001;139(1):70–4.
- Burstein D, Gray ML. Is MRI fulfilling its promise for molecular imaging of cartilage in arthritis? *Osteoarthritis Cartilage.* 2006;14(11):1087–90.
- Nieminen MT, Rieppo J, Toyra J, Hakumaki JM, Silvennoinen J, Hyttinen MM, Helminen HJ, Jurvelin JS. T2 relaxation reveals spatial collagen architecture in articular cartilage: a comparative quantitative MRI and polarized light microscopic study. *Magn Reson Med.* 2001;46(3):487–93.
- White LM, Sussman MS, Hurtig M, Probyn L, Tomlinson G, Kandel R. Cartilage T2 assessment: differentiation of normal hyaline cartilage and reparative tissue after arthroscopic cartilage repair in equine subjects. *Radiology.* 2006;241(2):407–14.
- Domayer SE, Kutscha-Lissberg F, Welsch G, Dorotka R, Nehrer S, Gabler C, Mamisch TC, Trattnig S. T2 mapping in the knee after microfracture at 3.0 T: correlation of global T2 values and clinical outcome—preliminary results. *Osteoarthritis Cartilage.* 2008;16(8):903–8.
- Grunder W, Wagner M, Werner A. MR-microscopic visualization of anisotropic internal cartilage structures using the magic angle technique. *Magn Reson Med.* 1998;39(3):376–82.
- Mosher TJ, Smith H, Dardzinski BJ, Schmithorst VJ, Smith MB. MR imaging and T2 mapping of femoral cartilage: in vivo determination of the magic angle effect. *AJR Am J Roentgenol.* 2001;177(3):665–9.
- Li X, Benjamin Ma C, Link TM, Castillo DD, Blumenkrantz G, Lozano J, Carballido-Gamio J, Ries M, Majumdar S. In vivo T(1rho) and T(2) mapping of articular cartilage in osteoarthritis of the knee using 3 T MRI. *Osteoarthritis Cartilage.* 2007;15(7):789–97.
- Trattnig S, Mamisch TC, Welsch GH, Glaser C, Szomolanyi P, Gebetsroither S, Stastny O, Horgner W, Millington S, Marlovits S. Quantitative T2 mapping of matrix-associated autologous chondrocyte transplantation at 3 Tesla: an in vivo cross-sectional study. *Invest Radiol.* 2007;42(6):442–8.
- Kurkijarvi JE, Mattila L, Ojala RO, Vasara AI, Jurvelin JS, Kiviranta I, Nieminen MT. Evaluation of cartilage repair in the distal femur after autologous chondrocyte transplantation using T2 relaxation time and dGEMRIC. *Osteoarthritis Cartilage.* 2007;15(4):372–8.
- Welsch GH, Mamisch TC, Domayer SE, Dorotka R, Kutscha-Lissberg F, Marlovits S, White LM, Trattnig S. Cartilage T2 assessment at 3-T MR

- imaging: in vivo differentiation of normal hyaline cartilage from reparative tissue after two cartilage repair procedures—initial experience. *Radiology*. 2008;247(1):154–61.
12. Quirbach S, Trattnig S, Marlovits S, Zimmermann V, Domayer S, Dorotka R, Mamisch TC, Bohndorf K, Welsch GH. Initial results of in vivo high-resolution morphological and biochemical cartilage imaging of patients after matrix-associated autologous chondrocyte transplantation (MACT) of the ankle. *Skeletal Radiol*. 2009;38(8):751–60.
 13. Domayer SE, Welsch GH, Stelzeneder D, Hirschfeld C, Quirbach S, Nehrer S, Dorotka R, Mamisch TC, Trattnig S. Microfracture in the ankle: clinical results and MRI with T2-mapping at 3.0 T after 1 to 8 years. *Cartilage*. 2011;2(1):73–80.
 14. Nehrer S, Domayer SE, Hirschfeld C, Stelzeneder D, Trattnig S, Dorotka R. Matrix-associated and autologous chondrocyte transplantation in the ankle: clinical and MRI follow-up after 2 to 11 years. *Cartilage*. 2011;2(1):81–91.
 15. Maier CF, Tan SG, Hariharan H, Potter HG. T2 quantitation of articular cartilage at 1.5 T. *J Magn Reson Imaging*. 2003;17(3):358–64.
 16. Pai A, Li X, Majumdar S. A comparative study at 3 T of sequence dependence of T2 quantitation in the knee. *Magn Reson Imaging*. 2008;26(9):1215–20.
 17. Glaser C, Mendlik T, Dinges J, Weber J, Stahl R, Trumm C, Reiser M. Global and regional reproducibility of T2 relaxation time measurements in human patellar cartilage. *Magn Reson Med*. 2006;56(3):527–34.
 18. Glaser C, Horng A, Mendlik T, Weckbach S, Hoffmann RT, Wagner S, Raya JG, Horger W, Reiser M. [T2 relaxation time in patellar cartilage—global and regional reproducibility at 1.5 tesla and 3 tesla]. *Rofo*. 2007;179(2):146–52.
 19. Mamisch TC, Hughes T, Mosher TJ, Mueller C, Trattnig S, Boesch C, Welsch GH. T2 star relaxation times for assessment of articular cartilage at 3 T: a feasibility study. *Skeletal Radiol*. 2012;41(3):287–92.
 20. Bittersohl B, Miese FR, Hosalkar HS, Mamisch TC, Antoch G, Krauspe R, Zilkens C. T2* mapping of acetabular and femoral hip joint cartilage at 3 T: a prospective controlled study. *Invest Radiol*. 2012;47(7):392–7.
 21. Apprich S, Welsch GH, Mamisch TC, Szomolanyi P, Mayerhoefer M, Pinker K, Trattnig S. Detection of degenerative cartilage disease: comparison of high-resolution morphological MR and quantitative T2 mapping at 3.0 Tesla. *Osteoarthritis Cartilage*. 2010;18(9):1211–7.
 22. Welsch GH, Apprich S, Zbyn S, Mamisch TC, Mlynarik V, Scheffler K, Bieri O, Trattnig S. Biochemical (T2, T2* and magnetisation transfer ratio) MRI of knee cartilage: feasibility at ultra-high field (7T) compared with high field (3T) strength. *Eur Radiol*. 2011;21(6):1136–43.
 23. Apprich S, Mamisch TC, Welsch GH, Bonel H, Siebenrock KA, Kim YJ, Trattnig S, Dudda M. Evaluation of articular cartilage in patients with femoroacetabular impingement (FAI) using T2* mapping at different time points at 3.0 Tesla MRI: a feasibility study. *Skeletal Radiol*. 2012;41(8):987–95.
 24. Guivel-Scharen V, Sinnwell T, Wolff SD, Balaban RS. Detection of proton chemical exchange between metabolites and water in biological tissues. *J Magn Reson*. 1998;133(1):36–45.
 25. Ward KM, Aletras AH, Balaban RS. A new class of contrast agents for MRI based on proton chemical exchange dependent saturation transfer (CEST). *J Magn Reson*. 2000;143(1):79–87.
 26. Ward KM, Balaban RS. Determination of pH using water protons and chemical exchange dependent saturation transfer (CEST). *Magn Reson Med*. 2000;44(5):799–802.
 27. Zhou JY, van Zijl PCM. Chemical exchange saturation transfer imaging and spectroscopy. *Prog Nucl Magn Reson Spectrosc*. 2006;48(2–3):109–36.
 28. Ling W, Regatte RR, Navon G, Jerschow A. Assessment of glycosaminoglycan concentration in vivo by chemical exchange-dependent saturation transfer (gagCEST). *Proc Natl Acad Sci U S A*. 2008;105(7):2266–70.
 29. Ayad S. The extracellular matrix factsbook. San Diego, CA: Academic; 1998. p. 301.
 30. Roughley PJ. The structure and function of cartilage proteoglycans. *Eur Cell Mater*. 2006;12:92–101.
 31. Roughley PJ, Lee ER. Cartilage proteoglycans—structure and potential functions. *Microsc Res Tech*. 1994;28(5):385–97.
 32. Reddy R, Li SC, Noyszewski EA, Kneeland JB, Leigh JS. In vivo sodium multiple quantum spectroscopy of human articular cartilage. *Magn Reson Med*. 1997;38(2):207–14.
 33. Borthakur A, Shapiro EM, Beers J, Kudchodkar S, Kneeland JB, Reddy R. Sensitivity of MRI to proteoglycan depletion in cartilage: comparison of sodium and proton MRI. *Osteoarthritis Cartilage*. 2000;8(4):288–93.
 34. Shapiro EM, Borthakur A, Dandora R, Kriss A, Leigh JS, Reddy R. Sodium visibility and quantitation in intact bovine articular cartilage using high field Na-23 MRI and MRS. *J Magn Reson*. 2000;142(1):24–31.
 35. Shapiro EM, Borthakur A, Gougoutas A, Reddy R. Na-23 MRI accurately measures fixed charge density in articular cartilage. *Magn Reson Med*. 2002;47(2):284–91.
 36. Krusche-Mandl I, Schmitt B, Zak L, Apprich S, Aldrian S, Juras V, Friedrich KM, Marlovits S, Weber M, Trattnig S. Long-term results 8 years after autologous osteochondral transplantation: 7 T gagCEST and sodium magnetic resonance imaging with morphological and clinical correlation. *Osteoarthritis Cartilage*. 2012;20(5):357–63.

37. Schmitt B, Zbyn S, Stelzeneder D, Jellus V, Paul D, Lauer L, Bachert P, Trattnig S. Cartilage quality assessment by using glycosaminoglycan chemical exchange saturation transfer and ^{23}Na MR imaging at 7 T. *Radiology*. 2011;260(1):257–64.
38. Eckstein F, Burstein D, Link TM. Quantitative MRI of cartilage and bone: degenerative changes in osteoarthritis. *NMR Biomed*. 2006;19(7):822–54.
39. Trattnig S, Domayer S, Welsch GW, Mosher T, Eckstein F. MR imaging of cartilage and its repair in the knee—a review. *Eur Radiol*. 2009;19(7):1582–94.
40. Welsch GH, Trattnig S, Hughes T, Quirbach S, Olk A, Blanke M, Marlovits S, Mamisch TC. T2 and T2*-mapping in patients after matrix-associated autologous chondrocyte transplantation: initial results on clinical use with 3.0-Tesla MRI. *Eur Radiol*. 2010;20(6):1515–23.
41. Trattnig S, Ba-Ssalamah A, Pinker K, Plank C, Vecsei V, Marlovits S. Matrix-based autologous chondrocyte implantation for cartilage repair: noninvasive monitoring by high-resolution magnetic resonance imaging. *Magn Reson Imaging*. 2005;23(7):779–87.
42. Trattnig S, Marlovits S, Gebetsroither S, Szomolanyi P, Welsch GH, Salomonowitz E, Watanabe A, Deimling M, Mamisch TC. Three-dimensional delayed gadolinium-enhanced MRI of cartilage (dGEMRIC) for in vivo evaluation of reparative cartilage after matrix-associated autologous chondrocyte transplantation at 3.0T: preliminary results. *J Magn Reson Imaging*. 2007;26(4):974–82.
43. Trattnig S, Welsch GH, Juras V, Szomolanyi P, Mayerhoefer ME, Stelzeneder D, Mamisch TC, Bieri O, Scheffler K, Zbyn S. ^{23}Na MR imaging at 7 T after knee matrix-associated autologous chondrocyte transplantation: preliminary results. *Radiology*. 2010;257(1):175–84.
44. Varma G, Kourtellis F, Madhurantakam A, Hackney DB, Lenkinski RE, Vinogradov E. Age-related assessment of intervertebral disc degeneration in the lumbar spine using gagCEST. *Melbourne: ISMRM*; 2012. p. 1460.
45. Kim M, Chan Q, Anthony MP, Samartzis D, Cheung KM, Khong PL. Chemical exchange saturation transfer and T2 mapping in subjects with intervertebral disc degeneration at 3 Tesla. *Melbourne: ISMRM*; 2012. p. 3331.
46. Singh A, Haris M, Cai K, Kassey VB, Kogan F, Reddy D, Hariharan H, Reddy R. Chemical exchange saturation transfer magnetic resonance imaging of human knee cartilage at 3 T and 7 T. *Magn Reson Med*. 2012;68(2):588–94.
47. Einstein A. Über die von der molekularkinetischen Theorie der Wärme geforderte Bewegung von in ruhenden Flüssigkeiten suspendierten Teilchen. *Ann Phys*. 1905;322(8):549–60.
48. von Smoluchowski M. Zur kinetischen Theorie der Brownschen Molekularbewegung und der Suspensionen. *Ann Phys*. 1906;326(14):756–80.
49. Tanner JE, Stejskal EO. Spin diffusion measurements: spin echoes in the presence of a time-dependent field gradient. *J Chem Phys*. 1965;42:288–92.
50. Le Bihan D, Breton E. Imagerie de diffusion in vivo par résonance magnétique nucléaire. *C R Acad Sci Paris*. 1985;301:1109–12.
51. Merboldt KD, Hancic W, Frahm J. Self-diffusion NMR imaging using stimulated echoes. *J Magn Reson*. 1985;64:479–86.
52. Taylor DG, Bushell MC. The spatial mapping of translational diffusion coefficients by the NMR imaging technique. *Phys Med Biol*. 1985;30:345–9.
53. Mlynarik V, Sulzbacher I, Bittsanksy M, Fuiko R, Trattnig S. Investigation of apparent diffusion constant as an indicator of early degenerative disease in articular cartilage. *J Magn Reson Imaging*. 2003;17(4):440–4.
54. Miller KL, Hargreaves BA, Gold GE, Pauly JM. Steady-state diffusion-weighted imaging of in vivo knee cartilage. *Magn Reson Med*. 2004;51(2):394–8.
55. Deoni SC, Peters TM, Rutt BK. Quantitative diffusion imaging with steady-state free precession. *Magn Reson Med*. 2004;51(2):428–33.
56. Kaiser R, Bartholdi E, Ernst RR. Diffusion and field-gradient effects in NMR Fourier spectroscopy. *J Chem Phys*. 1974;60:2966–79.
57. Le Bihan D. Intravoxel incoherent motion imaging using steady-state free precession. *Magn Reson Med*. 1988;7(3):346–51.
58. Merboldt KD, Bruhn H, Frahm J, Gyngell ML, Hancic W, Deimling M. MRI of “diffusion” in the human brain: new results using a modified CE-FAST sequence. *Magn Reson Med*. 1989;9(3):423–9.
59. Wu EX, Buxton RB. Effect of diffusion on the steady-state magnetization with pulsed field gradients. *J Magn Reson*. 1990;90(2):243–53.
60. Buxton RB. The diffusion sensitivity of fast steady-state free precession imaging. *Magn Reson Med*. 1993;29(2):235–43.
61. Patz S, Hawkes RC. The application of steady-state free precession to the study of very slow fluid flow. *Magn Reson Med*. 1986;3(1):140–5.
62. Merboldt KD, Hancic W, Gyngell ML, Frahm J, Bruhn H. Rapid NMR imaging of molecular self-diffusion using a modified CE-FAST sequence. *J Magn Reson*. 1989;82(1):115–21.
63. Mamisch TC, Menzel MI, Welsch GH, Bittersohl B, Salomonowitz E, Szomolanyi P, Kordelle J, Marlovits S, Trattnig S. Steady-state diffusion imaging for MR in-vivo evaluation of reparative cartilage after matrix-associated autologous chondrocyte transplantation at 3 tesla—preliminary results. *Eur J Radiol*. 2008;65(1):72–9.
64. Welsch GH, Trattnig S, Domayer S, Marlovits S, White LM, Mamisch TC. Multimodal approach in the use of clinical scoring, morphological MRI and biochemical T2-mapping and diffusion-weighted imaging in their ability to assess differences between cartilage repair tissue after microfracture therapy and

- matrix-associated autologous chondrocyte transplantation: a pilot study. *Osteoarthritis Cartilage*. 2009;17(9):1219–27.
65. Friedrich KM, Mamisch TC, Plank C, Langs G, Marlovits S, Salomonowitz E, Trattnig S, Welsch G. Diffusion-weighted imaging for the follow-up of patients after matrix-associated autologous chondrocyte transplantation. *Eur J Radiol*. 2010;73(3):622–8.
66. Bieri O, Ganter C, Welsch GH, Trattnig S, Mamisch TC, Scheffler K. Fast diffusion-weighted steady state free precession imaging of in vivo knee cartilage. *Magn Reson Med*. 2012;67(3):691–700.
67. Freed DE, Scheven UM, Zielinski LJ, Sen PN, Hürlimann MD. Steady-state free precession experiments and exact treatment of diffusion in a uniform gradient. *J Chem Phys*. 2001;119(9):4249–58.
68. Zur Y, Bosak E, Kaplan N. A new diffusion SSFP imaging technique. *Magn Reson Med*. 1997;37(5):716–22.
69. Deimling M. Method to determine the ADC coefficients in diffusion-weighted magnetic resonance imaging given use of steady-state sequences. US patent 6,891,373 B2; 2005.
70. Cho MH, Cho ZH. NMR diffusion coefficient mapping by use of fast steady-state free precession sequence. In: *Proceedings of Society of Magnetic Resonance in Medicine*, Amsterdam, The Netherlands; 1989. p 911.
71. Bieri O, Ganter C, Scheffler K. Quantitative in vivo diffusion imaging of cartilage using double echo steady-state free precession. *Magn Reson Med*. 2012;68(3):720–9.
72. Staroswiecki E, Granlund KL, Alley MT, Gold GE, Hargreaves BA. Simultaneous estimation of T(2) and apparent diffusion coefficient in human articular cartilage in vivo with a modified three-dimensional double echo steady state (DESS) sequence at 3 T. *Magn Reson Med*. 2012;67(4):1086–96.

Hip Magnetic Resonance Imaging

Kim, Y.-J.; Mamisch, T.C. (Eds.)

2014, XIII, 230 p. 199 illus., 80 illus. in color., Hardcover

ISBN: 978-1-4614-1667-8